Image Cover Sheet

CLASSIFICATION	SYSTEM NUMBER
UNCLASSIFIED	151970

TITLE

REFRACTION EFFECTS ON EO SYSTEM DETECTION RANGES IN COASTAL ENVIRONMENTS

System Number:

Patron Number:

Requester:

Notes: Paper #12 of Multipart document Sysnum #151751

DSIS Use only:

Deliver to: DK

Refraction Effects on EO System Detection Ranges in Coastal Environments

Denis Dion
Defence Research Establishment Valcartier
P.O. Box 8800, Courcelette, Québec
Canada G0A 1R0

1. SUMMARY

Atmospheric refraction can significantly affect the detection range performances of electro-optical (EO) systems against low-level targets in coastal environments. Negative air-sea temperature difference (ASTD) conditions, which produce subrefraction, impose an absolute limit of detection range shorter than the terrestrial horizon, while positive ASTD conditions, which produce superrefraction, allow radiation to propagate beyond the horizon. For subrefraction conditions, an approximate formula is given for estimating the detection range limit as a function of ASTD, wind speed and sensor-target elevations. Under superrefraction, the detectability is degraded by the refraction-induced ray spreading near the sea surface. This refraction loss, which depends on the weather conditions and the sensor-target elevations, is discussed.

2. INTRODUCTION

Under nonrefractive conditions - where the index of refraction of air can be considered invariant - EO radiation follows straight-line trajectories, and thence, the maximum detection ranges are limited by the terrestrial horizon. However, most of the time, the index of air rapidly varies with elevation near the sea surface and, depending on the conditions, this variation can significantly affect the detection range performances of EO systems due to the bending of rays, as introduced by Dion and Leclerc few years ago [1].

In the marine surface layer, the vertical variation of the index dominates, and in most cases the horizontal variations can be neglected over the EO detection ranges. The refraction conditions can be divided into two families which are characterized by the sign of the vertical index variation (gradient) at the sea surface: subrefraction conditions, when the gradient is positive, and superrefraction conditions, when the gradient is negative. Figure 1 shows ray diagrams for EO systems under typical sub- and superrefraction conditions. The dashed line shows the range limitation due to the earth curvature (versus target height), hereafter denoted horizon-limited range (HLR). For a given sensor and target height, HLR can be obtained using:

$$\begin{aligned} \mathrm{HLR} &= \sqrt{2a}\left[\sqrt{h_s}+\sqrt{h_t}\right] x\, 10^{-3} \\ &\approx 3.57\left[\sqrt{h_s}+\sqrt{h_t}\right] \end{aligned} \qquad (1)$$

where HLR is expressed in kilometers while the sensor height h_S, the target height h_t and the earth radius a are expressed in meters ($a \approx$ 6 370 000 m) [2].

As shown in Fig. 1, under subrefraction, the upward bending of the radiation imposes an absolute limit of detection range shorter than HLR. In contrast, under superrefraction conditions, the rays are bent downward, making possible detection of targets well beyond the horizon. The ray crossing and the caustic observed in the subrefraction diagram are due to the exponential nature of the index gradient near the surface [1].

In the IR and the visible, the index gradient of air is dominantly dependent upon the temperature gradient in the operational windows of EO systems (where absorption is low). As the index gradient is inversely proportional to the temperature gradient, negative temperature gradients produce subrefraction, whereas positive temperature gradients produce superrefraction. The negative surface temperature gradient conditions (subrefraction) are by far the most frequent ones in open sea. In coastal environments, they normally prevail when maritime air is present (e.g. when the atmospheric conditions are driven by the sea wind). The positive surface temperature gradients (superrefraction) are infrequent on a world average basis. However, near the coasts, depending on the region of the world and the season, their occurrence can be very significant when the air mass is continental; more precisely, they are likely to occur when warm continental air is blown, from the land, over cool water.

In this paper, the effects on detection range performances are discussed separately for the two families of conditions, starting with subrefraction. Under subrefraction conditions, good estimates of the refraction-limited ranges can be obtained using approximate formulae fitted on calculated values. A formulae expressed as a function of ASTD and wind speed is presented in Section 3. In Section 4, the loss of detectability produced by refraction under superrefraction is discussed.

3. MAXIMUM INTER-VISION RANGES UNDER SUBREFRACTION CONDITIONS

For subrefractive conditions, we use the expression maximum inter-vision range (MIVR) to denote the absolute detection range limit imposed by refraction for a given sensor and target height. In Fig. 1, the caustic boundary constitutes, at the same time, the MIVR versus target height curve. EO detection beyond these ranges is physically impossible as no rays can go beyond. In a nonrefractive atmosphere, the MIVRs would correspond exactly to the HLRs (see Fig. 1).

Paper presented at the Sensor and Propagation Panel Symposium on "Propagation Assessment in Coastal Environments" held in Bremerhaven, Germany 19-22 September 1994.

Using the air-sea temperature difference (ASTD) to simply characterize the atmosphere's vertical temperature variation, Fig. 2 shows the MIVR variation relative to HLR with respect to ASTD for various wind speeds. These results are for a sensor and a target located 10 m above the sea surface. As given by (1), in this case, the HLR is 22.6 km. In the graphic, the points were obtained by using the Canadian WKD marine boundary layer model [2] - a model which gives vertical refractivity profiles - in conjunction with ray tracing. The relative humidity is taken to be 80% and the reference heights for the temperature and wind speed are 12 and 19.5 m, respectively, which correspond to the standard measurement elevations on board a ship. The graphic shows that significant decrease of detection range can be caused by refraction when ASTD and wind speed are relatively large; for instance, as shown in the figure, for the geometry considered, the detection range limit is about 22% of HLR (thus MIVR = .22 x HLR = 17.6 km) when ASTD is -4 °C and the wind speed is 15 m/sec.

The WKD-based predictions of MIVRs have so far proved appreciably accurate over a diversity of ASTD, wind speed conditions and target-sensor elevations [4] [5]. The MIVR predictions, as shown in Fig. 2, can be considered valid for low-level targets unless the atmosphere is highly inhomogeneous along the propagation path. In most cases, the horizontal variations of the atmospheric conditions over refraction-shortened detection ranges are not likely to significantly affect MIVR predictions. In Ref. [5], predictions made using a single vertical index profile proved satisfactorily accurate even under the experimented inhomogeneous conditions. The MIVR predictions shown in Fig. 2 apply in the visible as well as in the IR 3-5 and 8-12 μm windows as the refractivity gradients can be considered constant over the operational wavebands of EO systems.

In Fig. 2, one notes that MIVRs slightly greater than HLR are obtained for 0 °C ASTD. This light superrefraction effect is due to the atmospheric pressure gradient [1]. We also note that MIVR variations tend to converge as the wind speed increases. Although not shown in Fig. 2, the MIVRs become almost invariant with respect to wind for speeds greater than 15 m/sec. Furthermore, we note that the MIVR variations can be as much sensitive to wind as to ASTD depending on the conditions.

The apparent smooth parabolic-like MIVR variations observed versus ASTD for the different wind speeds allows one to derive approximative formulae for estimating MIVR. Curves in Fig. 2 are polynomial fits on MIVR calculations for the different wind speeds considered. In a second step, fits can be performed over wind speeds to obtain the coefficients of the MIVR-versus-ASTD functions for any wind speed. This second fit (over wind speeds) includes a difficulty due to the discontinuity caused by the crossing of MIVR curves at mid-wind velocity (about 9.5 m/sec) for low ASTDs, as observed in Fig. 2.

Having a MIVR solution for one sensor-target geometry, the MIVRs for any sensor height-target height combinations can be found by exploiting the near-linear variation of MIVR with respect to the height parameter, H:

$$H = \sqrt{h_s} + \sqrt{h_t} \qquad (2)$$

where h_S and h_t are the sensor and the target heights expressed in meters, respectively. This linear variation is shown in Fig. 3a and b which present MIVR with respect to H for various ASTDs and wind velocities. Figure 3b, which shows the curves against normalized axis, outlines the discrepancies between slopes. The slope variation can lead to significant MIVR differences for large ΔHs, and thence, it must be taken into account in the calculations of MIVRs.

Therefore, one can look for describing MIVR variations under subrefraction conditions with a function of ASTD and wind velocity (neglecting the pressure and humidity gradient effects) borrowing the form of the effective-earth-radius expression originally developed for RF applications [2]. However, unlike the original form which was derived assuming linear index gradients, a factor, Γ, is required to account for the sensor height-target height geometry effect discussed above. Thence, the general expression for MIVR can write:

$$MIVR = K_0 \sqrt{\frac{1}{1 + \Phi(\Delta, \omega)}} \cdot \Gamma(H, \Delta, \omega) \qquad (3)$$

where MIVR is expressed in kilometers, Δ is ASTD in degrees, ω is the wind speed in m/sec, H is given by (2) and K_0 is a constant = 22.405. Expressions for Φ and Γ are given in APPENDIX.

Figure 4 exhibits the distribution of the errors obtained running the proposed expression (3) over 200 cases, for ASTDs ranging from 0 to -8 degrees; wind speeds ranging from 1 to 20 m/sec and for sensor and target heights going from 5 to 20 m. We note that errors obtained are less than 0.4 km in 90 % of the cases considered. This accuracy is certainly sufficient for EO system studies where other factors, often more significant factors, are much less accurately known (e.g. transmittance, sea and sky background radiances, etc.). It is interesting to note that 0.5 km corresponds approximately to the predictions errors obtained from the MAPTIP experiment under the best conditions [5]; under the worst horizontally varying conditions experimented at MAPTIP, the prediction errors were about twice greater. Calculations of MIVRs using (3) can be very useful in target detection simulations, for instance, for screening out quickly physically undetectable targets without getting through profiles computations and ray tracing.

4. REFRACTION LOSSES UNDER SUPERREFRACTION CONDITIONS

Under typical superrefraction conditions, ray diagrams show virtually no distinct range limitations, as shown in Fig. 1, and so the MIVR concept does not apply. However, one notes that the ray density (thence, the intensity of the radiation) decreases rapidly near the surface from about the horizon, which produces a loss of detectability. The rate of decrease of the radiation intensity versus range depends on the refractive conditions and the sensor-target elevations.

To describe this refraction loss, one can define a new parameter, hereafter called "refractance", which gives the radiation intensity (due to the geometrical spreading) relative to $1/R^2$, which is normally assumed in any system studies. Like for the MIVR, the refractance is not wavelength dependent. In the calculation of subpixel target detection, one can show that the refractance, ρ, directly affects the contrast, C, and so the signal-to-noise ratio, SNR:

$$SNR = \frac{C}{NEI} = \rho \frac{A_t}{R^2}[N_t' + N_p - N_b'] \qquad (4)$$

where:
NEI is the noise equivalent irradiance ($W/m^2/sr$);
A_t is the apparent target area (m^2);
R is the slant range between detector and target (m);
N_t' is the attenuated target irradiance ($W/m^2/sr$);
N_p is the path radiance ($W/m^2/sr$); and,
N_b' is the attenuated background irradiance ($W/m^2/sr$).

Figure 5 shows the refractance versus range for two different superrefraction conditions, for a sensor located 22.5 m above water. The HLR is also shown. When refraction is neglected, ρ is usually considered equal to 1 for $R <$ HLR and equal to 0 for $R >$ HLR. The refractance curves in Fig. 5 were obtained using WKD in conjunction with the DREV ray tracing technique which incorporates ray-intensity calculation [6].

During a measurement campaign conducted in Sylt (Germany) jointly with the Netherlands and Germany in June 1992, tracking of targets moving away from the observer was experimented under the conditions considered for the solid line in Fig. 5 [7]. The arrow indicates where the target located 2.8 m above water was lost during the tracking session. Note that, in this case, the maximum detection range is about 1.5 x HLR, which is significant. This result does demonstrate that limiting detection at HLR, as it is usually done in EO system studies, may lead to excessively pessimistic performance predictions, especially for coastal environments where these conditions can be frequent. It is worth mentioning that clear and warm weathers, favorable for extended detection ranges, prevailed during daytime for more than 8 consecutive days during the Sylt campaign [8].

Figure 5 also shows the refractance under a different atmospheric condition (dashed line) where the refractance decreases more slowly. One shall be careful in interpreting these curves and shall not conclude that the maximum detection range would be necessarily significantly greater in the case of the dashed curve. It must be stressed that the graphic presents exclusively the effect of refraction. Radiation that reaches low-level targets beyond the horizon has to propagate very near the surface over long distances, and so the detection range is likely to be dominantly dependent upon the surface aerosols density under most conditions.

A rigorous experimental validation of refractance prediction curves is difficult and tricky. In particular, the assumption of horizontal homogeneity, which is made here, may lead to sizeable errors especially when long ranges are considered. Evaluating refractance may also imply that all complementary factors affecting the contrast, especially the transmittance, are accurately known. However, the over-spreading of rays that occurs near the surface under superrefraction produces an image compression and the compression ratio is an indirect, though valid, measurement of ray intensity. Although very few measurements of compression ratio have been made so far, they have been in agreement with predictions when the conditions could be assumed homogeneous. An example was presented by Dion et al. a few years ago [4].

To give indications of the refractance variation with respect to the strength of the superrefraction conditions, Fig. 6 shows the predicted ranges where the refractance reaches 0.8 and 0.5, respectively under various ASTD and wind speed conditions. Note that some refraction losses are obtained at ranges less than the horizon. This can also be observed in Fig 5. Long detection range capability due to refraction implies in turn some losses of detectability at shorter distances.

Plots for two refractances, as given in Fig. 6, inform about the rate of decrease of the refractance versus range with respect to the ASTD and wind speed conditions. We see that the sensitivity to wind increases rapidly with ASTD. We also note that, as the wind speed decreases, the potential-range performances increase very rapidly. However, it must be mentioned that the stability length, the Monin-Obukhov stability length, L, which can be seen as a measure of the model validity, decreases with decreasing wind speed. In Fig. 6, curves stop at conditions where L gets lower than 15 m; this is an arbitrary criterion since good profile predictions can be obtained for lower L values.

The effect of sensor and target elevations is in relation to the "optical" duct height. As defined in the RF, the duct height corresponds to the elevation where the modified air refractivity goes to a minimum (or, in other words, where its gradient passes through 0). Figure 7 shows the duct height for the visible and the IR versus ASTD and wind speed. Here again, curves stop at conditions where the stability length gets lower than 15 m. Like in the RF, better refractance performances is obtained when both the sensor and the target are below the duct height. However, one notes that, for EO systems, under most conditions the duct height is much lower than the sensor heights of interest for ship defence applications. Moreover, it has to be mentioned that when the target is slightly above the duct, where a "hole" is produced, the refractance falls off rapidly.

5. CONCLUSIONS

In coastal environments, the near-sea surface refraction effects on detection range of low-level targets can be significant, and so, techniques are required to efficiently take them into account in the calculation of detection range performances of EO systems. Subrefraction conditions, that are likely to occur when the air mass is maritime, induces an abrupt detection range limit which can be reliably predicted and readily estimated using

approximative formulae; an expression was derived as a function of ASTD and wind velocity. Warm continental air blowing over cool coastal water can produce superrefraction which can lead to significantly extended detection range. Under these conditions, assuming that the detection ranges are limited by the horizon (as it is usually done) can greatly underestimate the system performances. The use of "refractance" has been proposed to take into account the refraction losses under superrefraction conditions in the calculation of detection ranges of EO systems.

6. REFERENCES

1. Dion, D. and Leclerc, B., "Investigation of the Air Refractivity Effects on IR Sensors in the Marine Boundary Layer", DREV-R-4570/90, August 1990.

2. Skolnik, M.I., "Introduction to Radar Systems", McGraw-Hill Book Company, 1970.

3. Low, T.B. and Hudak, D.R., "Final Report on the Development and Testing of a Marine Boundary Layer Model", KelResearch Corp., Report under DSS contract #W7701-8-2419/01-XSK, September 1990.

4. Dion, D., Forand, J.L., Fournier, G.R. and Pace, P., "Experimental Data on Near-Surface Refraction Effects at Optical Wavelengths", Optics of the Air-Sea Interface: Theory and Measurements, Lesland Estep, Editor, Proc. SPIE 1749, 1993.

5. Forand, J.L., Dion, D. and Beaulieu, J., "MAPTIP: Canada's Measurements of Refraction Effects", presented at 2nd Symposium of the AGARD Sensor and Propagation Panel on "Propagation Assessment in Coastal Environments", Bremerhaven, Germany, 19-22 September, 1994.

6. Blanchard, A., "Phase and Intensity Ray Tracing to Study the Propagation of Coherent Radiation in the Atmosphere and other Media", DREV-R-4699/93, January 1993.

7. Dion, D. and Beaulieu, J., "Sylt '92 Campaign: The Complementarity of Radar and EO Sensors", private communication, December 1993.

8. De Leeuw, G., Neele, F.P. and Van Eijk, A.M.J., "IR/RF Refractivity Profiles over Coastal Water", presented at 2nd Symposium of the AGARD Sensor and Propagation Panel on "Propagation Assessment in Coastal Environments", Bremerhaven, Germany, 19-22 September, 1994.

7. APPENDIX: APPROXIMATE MIVR FUNCTION

Under subrefraction conditions, equation (3) can be used for estimating MIVR, where:

$$\Phi = \alpha\Delta^2 + \beta\Delta + \gamma \qquad (5)$$

where:

$$\begin{aligned} \alpha &= -10^{-3}\left(2.159 + 8.4\ log(\omega)\right) && ;\omega < 9.5\ m/sec \\ &= -10^{-2}\left(1.3921 - 0.037454\ \omega\right) && ;\omega \geq 9.5\ m/sec \end{aligned} \qquad (6)$$

$$\begin{aligned} \beta &= -10^{-2}\left(1.5 + 3.6\omega - 0.19\ \omega^2\right) && ;\omega < 9.5\ m/sec \\ &= -10^{-1}\left(2.184 - 0.0098395\ \omega\right) && ;\omega \geq 9.5\ m/sec \end{aligned} \qquad (7)$$

$$\begin{aligned} \gamma &= 0 && ;\omega < 9.5\ m/sec \\ &= -0.02 && ;\omega \geq 9.5\ m/sec \end{aligned} \qquad (8)$$

where Δ is the air-sea temperature difference in degrees and ω is the wind speed in m/sec. For wind speeds less than 0.5 m/sec, the value 0.5 m/sec shall be used in the calculation.

In (3), the function Γ, which accounts for the effect of the sensor and target heights, is given by:

$$\Gamma = \left(H^* - 1\right)\left(1.1 - S\cdot\Delta\right) + 1 \qquad (9)$$

where:

$$H^* = \frac{H}{6.3246} \qquad (10)$$

where H is given by (2) and:

$$S = 0.0175 + 0.0375\left[1 - exp\left(-(\omega-1)/2.5\right)\right]. \qquad (11)$$

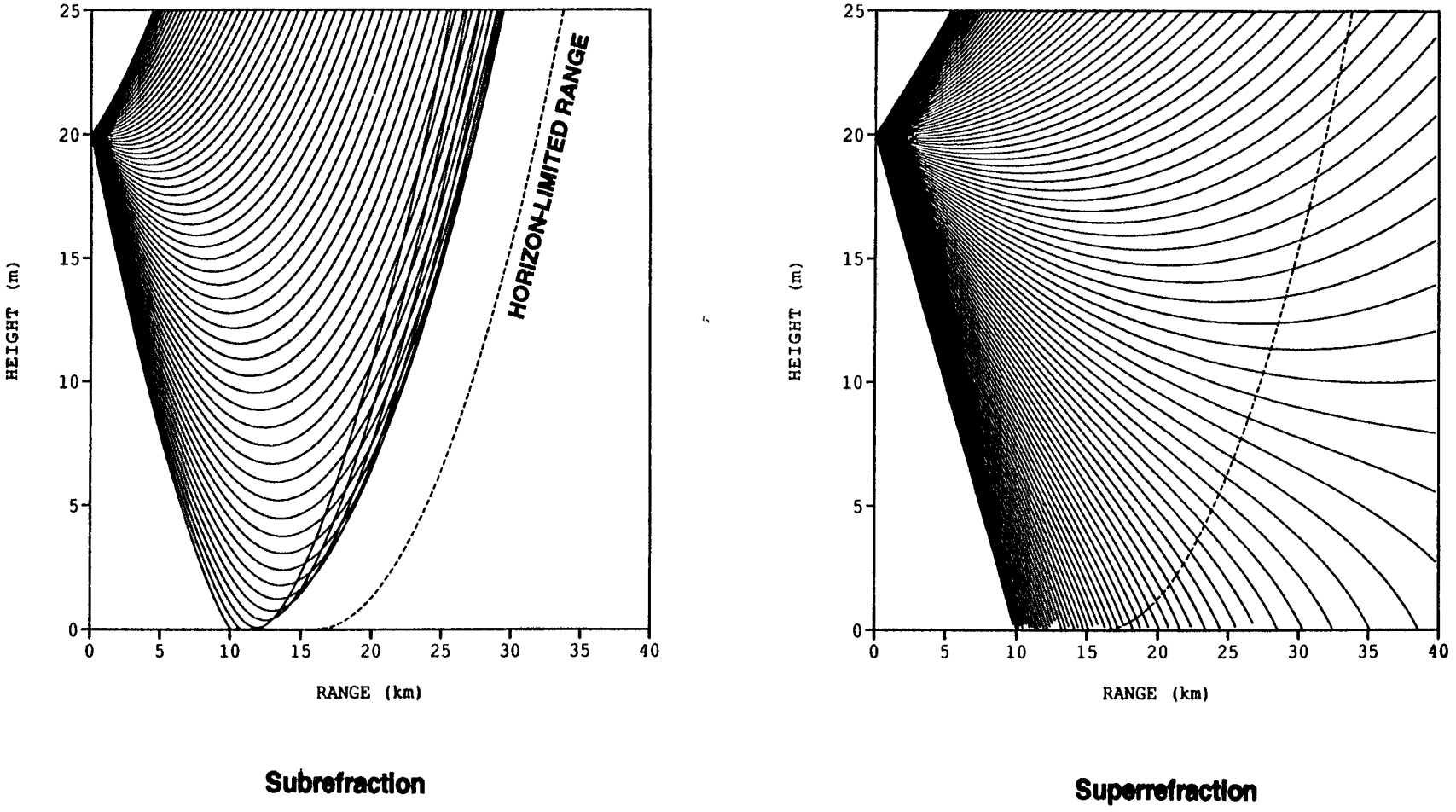

Fig. 1 - Ray diagram for typical sub- and superrefraction conditions

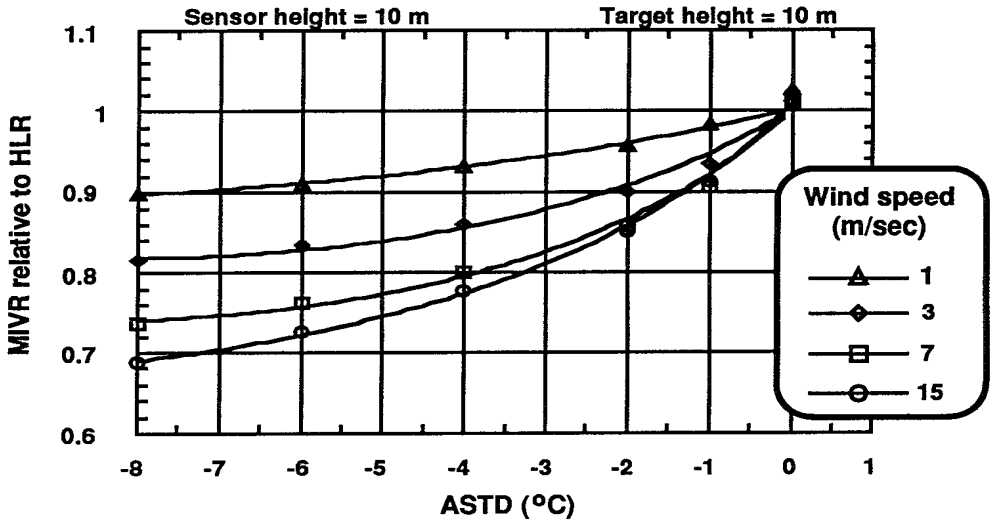

Fig. 2 - MIVR (relative to HLR) versus ASTD for different wind speed conditions

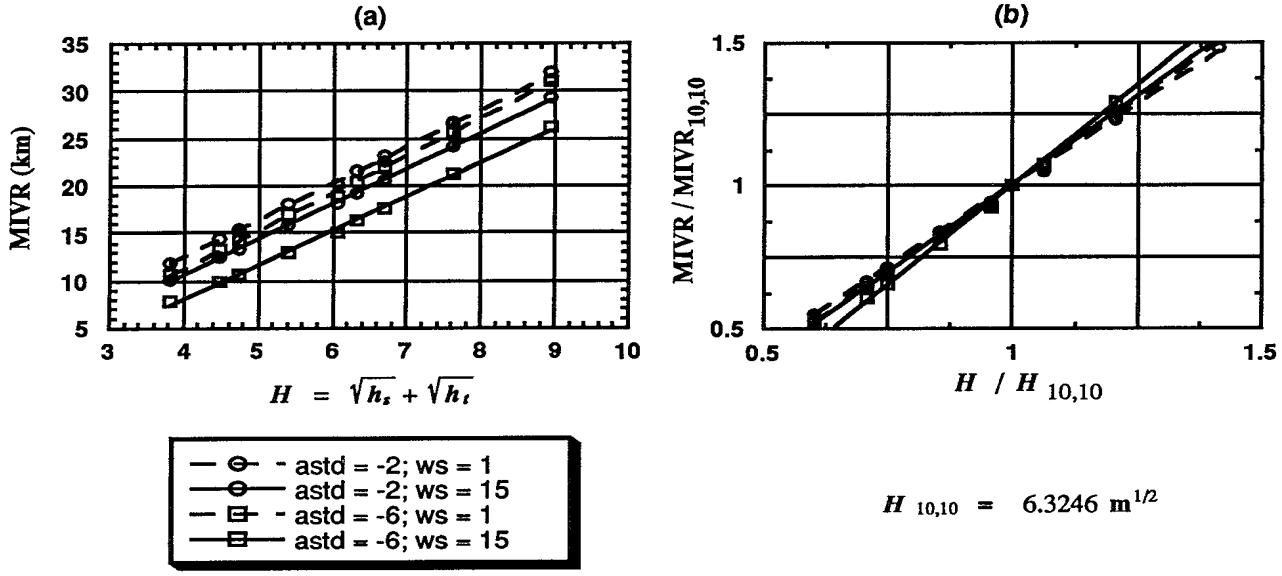

Fig. 3 - MIVR with respect to the sensor-target height parameter *H* for various ASTD and wind speed conditions; the wind speed (ws) is in m/sec; *H* (10,10) and MIVR(10,10) are the *H* and MIVR values for a sensor and a target located 10 m above the sea surface

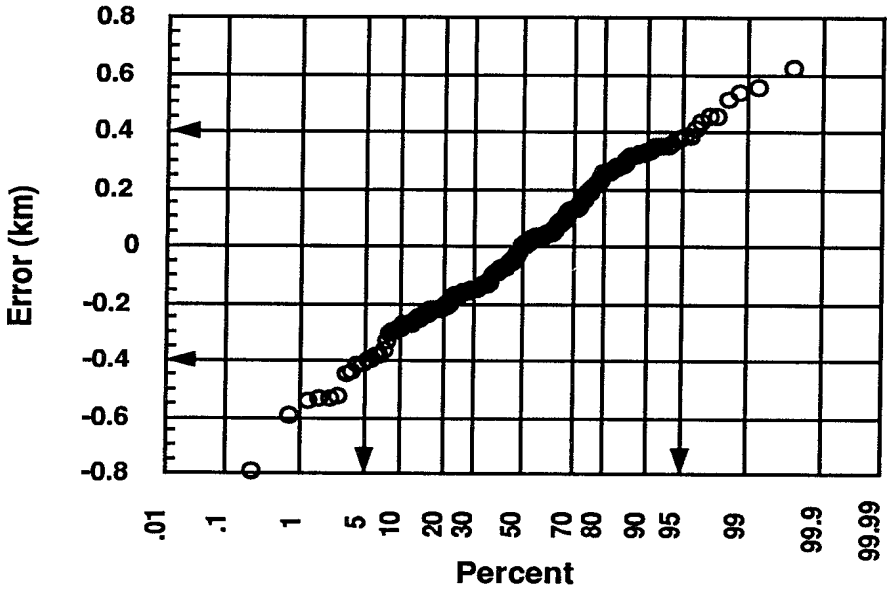

Fig. 4 - Distribution of the errors obtained using the approximate MIVR expression

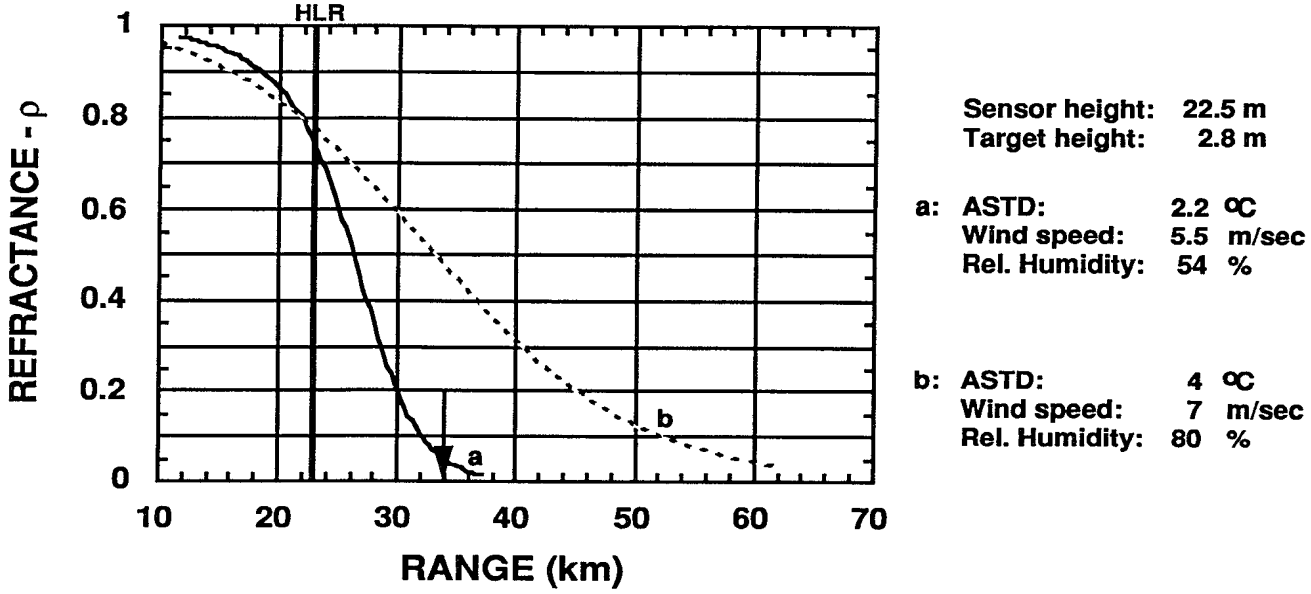

Fig. 5 - Refractance versus range for two refractivity conditions

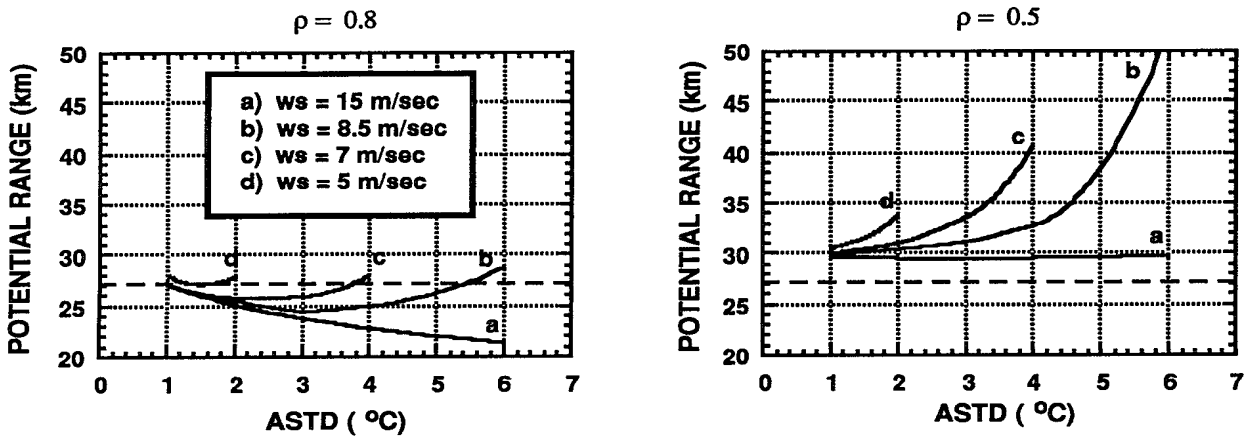

Fig. 6 - Potential range performance versus ASTD and wind speed for ρ = 0.5 and 0.8, respectively; the sensor height is 20 m and the target height is 10 m; ws stands for wind speed

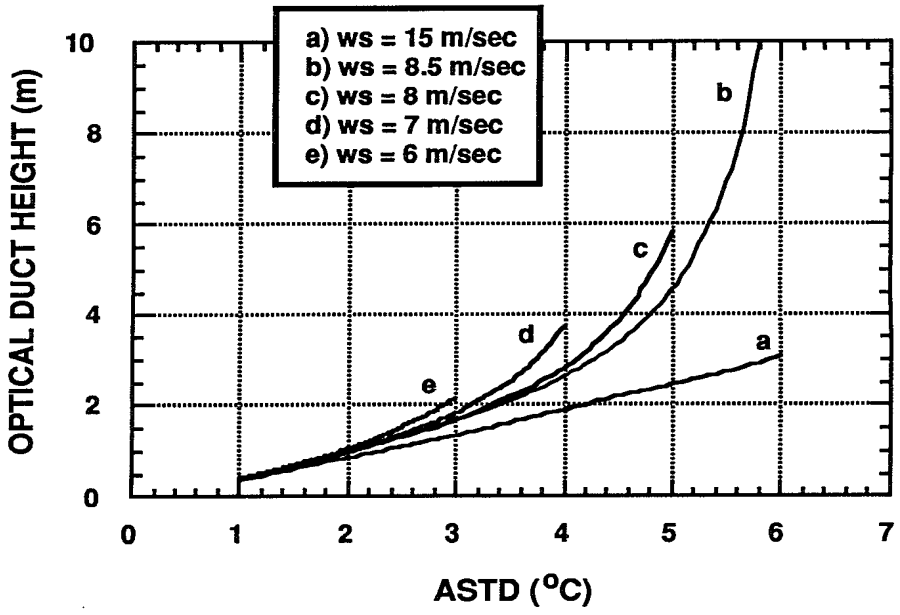

Fig. 7 - "Optical" duct height versus ASTD for different wind speed conditions; ws stands for wind speed

DISCUSSION

D. DOCKERY

You have discussed cases where upward ray bending causes MIVRs to be shorter than the geometric horizon, and cases where downward ray bending causes propagation beyond the horizon. Are there not also cases between these two extremes?

AUTHOR'S REPLY

Under non-refractive conditions (i.e. when the refractive index of air can be considered spatially invariant), rays are straight lines and MIVRs correspond to the geometrical horizon. Sub-refraction (produced when ASTD < 0 °C) prevents rays from reaching the horizon due to the upward bending phenomenon. When the ASTD is positive (theoretically for an ASTD greater than about -0.5°C due to the pressure gradient effect) rays go beyond the horizon. In general, under significantly positive ASTD conditions, propagation well beyond the horizon is made possible and the MIVR concept does not apply; in this case, the use of "refractance" is proposed to describe the refraction effects. However, for slightly positive ASTD conditions (ASTD $\approx$ 1.5°), there are limit conditions which make the evaluation of both the MIVR and the refractance difficult (potentially inapplicable).